

Mechanical property variance amongst vertical fused filament fabricated specimens via four different printing methods

Richard Davies, Nan Yi,^{*}  Paul McCutcheon and Oana Ghita

Abstract

Amongst additive manufacturing processes, fused filament fabrication (FFF) is one of the most affordable and cost-efficient technologies that can produce complex shaped components with an increasing number of printable polymers such as the polyaryletherketone family, polyetherimide and polyphenylene sulfide. Despite the gain in popularity, there is a lack of standardisation in specimen preparation and mechanical testing of FFF samples. This study investigates the effect of different methods of printing vertical tensile specimens on the mechanical properties when the material and the printing parameters are fixed. A slow crystallising polyetherketoneketone grade was selected as the printing material to exclude the effect of crystallisation on the interlayer bonding strength, leaving the temperature-dependent amorphous molecular diffusion across the layers as the governing mechanism. Vertical tensile specimens made by four printing methods – individually printed, machined and connected (based on ISO 527-2-1A and ISO 527-2-1BA) – were assessed. Individually printed vertical specimens were found to have the highest mean tensile strength, owing to the high level of diffusion induced by the very short layer time. The strengths of specimens printed via the other three methods are less sensitive to the effect of layer time, due to the lower rate of change during cooling and its relationship with the local temperature at the interlayer surface. This study highlights the importance of the disclosure of FFF printing methods along with any reported mechanical data.

© 2021 The Authors. *Polymer International* published by John Wiley & Sons Ltd on behalf of Society of Chemical Industry.

Keywords: polyaryletherketone; fused filament fabrication; mechanical testing; printing method

INTRODUCTION

Material extrusion of polymers, commonly known as fused filament fabrication (FFF), is one of several recognised methods of additive manufacturing (AM), picking up speed and reliability as well as a wider range of high-performance materials available. The ASTM International Committee F42 on Additive Manufacturing Technologies standardised the FFF technology with the term material extrusion and the following definition: ‘an additive manufacturing process in which material is selectively dispensed through a nozzle or orifice’.¹

The process has been published in multiple research papers with a vast range of polymeric materials^{2–5} and their compounds.⁶ Among the printable polymers, the polyaryletherketone (PAEK) family attracts increasing attention due to its superior mechanical properties and good biocompatibility.

Depending on the maturity of the AM system, some manufacturers provide a qualified material and parameter set which they have tested in-house and proven mechanical data. As such, Stratasys offers proprietary materials with fixed processing conditions to ensure components meet the published mechanical values when produced on their AM systems. One example would be Stratasys Ultem 1010.⁷ Alternatively, material manufacturers offer guideline mechanical values subject to processing conditions and machine quality, such as Luvocom PET-CF.⁸

Much of the published research into FFF process optimisation focuses on the variability of process parameters and how these can be optimised for specific mechanical values such as maximum tensile stress or flexural stress and typical test samples produced in the XY (flat) and XZ (edge) orientations.^{2–5}

The maximum tensile stress of specimens aligned along the ZX (vertical) axis offers a good indication of the layer to layer bonding strength of the process and of the material and is often significantly lower than the maximum tensile stress in the XY and XZ orientation, highlighting the anisotropy of the FFF process compared to other polymer processes such as injection moulding. Figure 1 displays the three notations of build orientation.

Tensile stress and Young’s modulus are two of the most commonly analysed mechanical properties when evaluating and optimising FFF polymer machines. Mechanical datasheets provided by machine manufacturers often focus on XY and XZ tensile values with only few providing Z tensile values. However, end user demands are driving change with respect to complete technical data sheets for all orientations.

^{*} Correspondence to: N Yi, College of Engineering, Mathematics and Physical Sciences, University of Exeter, Exeter, EX4 4QF, UK. E-mail: n.yi@exeter.ac.uk

College of Engineering, Mathematics and Physical Sciences, University of Exeter, Exeter, UK

The established test standards only provide limited guidance on the characterisation of AM specimens. The European Standard EN ISO 527-2:2012 'Plastics – Determination of tensile properties – Part 2: Test conditions for moulding and extrusion plastics' sets out the conditions for sample types and manufacturing conditions,⁹ although not specific for AM. The standard states that 'wherever possible, the test specimens shall be dumb-bell-shaped types 1A and 1B as shown in Fig. 1 and Table 1. Type 1A shall be used for directly injection-moulded multipurpose test specimens, type 1B for machined specimens.' It also states that 'test specimens with machined surfaces will not give results comparable to specimens having non-machined surfaces'. The final important part of the standard mentions that 'results obtained from small specimens are not comparable with those obtained from type 1 specimens'.

Whilst some technical datasheets list a testing standard or number of samples tested, we have found limited information specifying the method of manufacturing the specimens from which the data are recorded. The only study specifying the preparation method was defined for ULTEM⁷ within the printer's proprietary control software from which the specimens are built and tested. This includes reference to number of specimens, support material methodology and the inclusion of a sacrificial tower built to the height of the model.¹⁰ Other manufacturers have published just the test method identification and the value with no information on number of samples, construction methods or printing

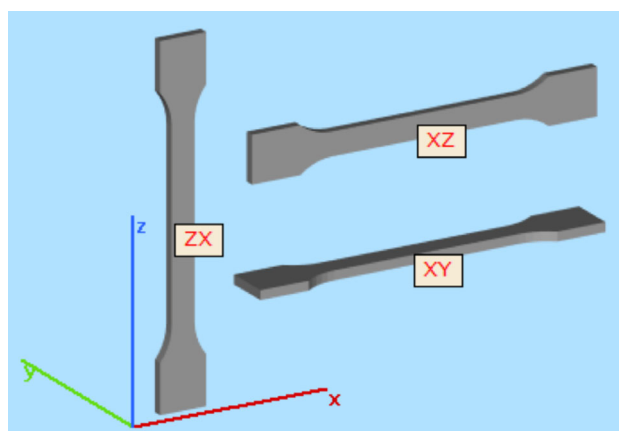


Figure 1. Illustration of three build orientations.

Table 1. Printing parameters for fabricating all specimens

Printing parameters	Method 1	Methods 2, 3, 4
Fan speed, %	50	0
Layer thickness, mm		0.15
Nozzle diameter, mm		0.4
Filament diameter, mm		1.75
Nozzle temperature, °C		380
Chamber temperature, °C		65
Platform temperature, °C		110
Number of contours		2
Infill, %		100
Perimeter velocity, mm s ⁻¹		20
Infill velocity, mm s ⁻¹		30
Top/bottom layer velocity, mm s ⁻¹		10

strategy.¹¹ Moreover, some manufacturers provide only a material datasheet but not the printed component datasheet.¹² The lack of information is one of the incentives to conduct this study.

Gebisa and Lemu¹³ conducted a full factorial design of experiment for the tensile properties of ULTEM 9085 focusing on five process parameters: air gap, raster width, raster angle, contour number and contour width. Wu *et al.*¹⁴ investigated the effect of layer thickness and raster angle on the mechanical properties of polyetheretherketone (PEEK) and acrylonitrile butadiene styrene (ABS) in a comparative study. Zhao *et al.*¹⁵ proposed two mathematical models to predict tensile strength and Young's modulus following their investigation into the effect of printing orientation and layer thickness. However, what is missing from the current published research is a standardisation of the sample manufacture which should be considered before investigation into the process parameter variables. For example, Rinaldi *et al.*¹⁶ printed ASTM D638-Type V vertical (Z) tensile specimens individually with a circular support structure at the bottom. Meanwhile, Arif *et al.*¹⁷ printed four ISO 527-2-1BA type vertical (Z) tensile specimens in a single fabrication sequence. Although both studies printed Virectex PEEK450 via Indmatec printers, the former reported a Z tensile strength of 19.6 MPa whilst the latter reported a Z tensile strength of 9.99 MPa. The results of these incommensurable different printing strategies weaken the arguments made by comparing mechanical data from various sources.¹⁸

This study attempts to investigate the effect of tensile specimen manufacture on the Z mechanical performance whereby the material and process parameters are fixed and only the methods of tensile specimen preparation are changed.

METHODOLOGY

FFF process

Due to the nature of the FFF process, manufacturing Z tensile specimens is more challenging, and several methods have been employed to successfully construct valid test specimens. This study proposed four methods to construct Z tensile ISO 527-2-1A and ISO 527-2-1BA specimens, respectively (Fig. 2). Ten specimens for each design were manufactured and tested.

Method 1 involves an individual Z specimen, unsupported. Depending on the specific AM system and the heating environment,

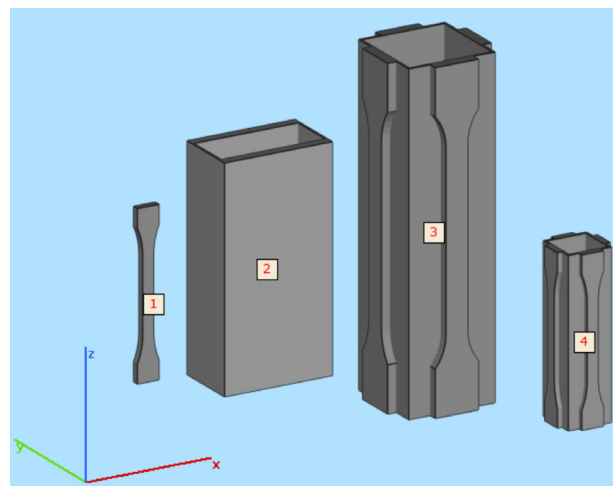


Figure 2. The four methods proposed for the manufacture of Z tensile samples.

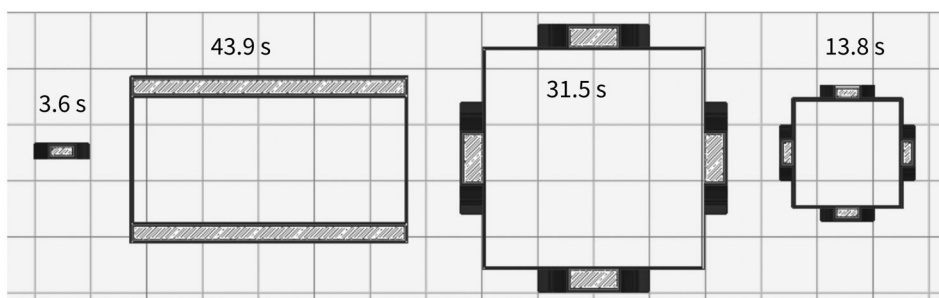


Figure 3. Cross-section through the gauge-length of all specimens showing the toolpaths of the two contours and alternative hatching at 100% infill. The corresponding layer times are marked in the figure.

it is possible to build an individual tensile specimen type 1BA in the vertical (Z) axis. Some systems will require the addition of a support structure (scaffold), which may be a secondary material.

In method 2, as a first step, a wall or tower geometry with matching thickness to the tensile specimen thickness was built, and then the specimen geometry was machined from the vertical walls.

In method 3 continuously connected specimens were formed. Various geometries can be constructed where the tensile specimen is connected to a thin wall structure, enabling the manufacture of multiple specimens that self-support during the AM process.

Method 4 is similar in design to method 3 but using type 1BA specimens.

The specimens were manufactured using a 3DGence Industry F340 FFF system (Przysowice, Poland) in Kimya PEKK-A (polyetherketoneketone) material (Nantes, France) with identical processing parameters except for method 1 which required the use of the part cooling fan due to the short layer time (see Table 1). Without the cooling fans the deposited polymer remained above its glass transition temperature during construction, leaving insufficient rigidity to support the next printed layer, resulting in a deformed gauge area. Layer time is the time interval between printing consecutive layers. The cross-sections of specimens from the four methods in the gauge-length zone are displayed in Fig. 3, with the corresponding layer times. ESM-10 soluble support material (Przysowice, Poland) was used to build a raft structure below the specimens. All filaments were stored under 45 °C for at least 24 h before printing. Method 3 specimens were machined using an Openbuilds Benchtop Router (Monroeville, USA) at a cutting speed of 3 mm s⁻¹.

Mechanical test

Tensile tests were performed to characterise the effect of sample manufacture using a 20 kN capacity standard tensile/compression machine (Shimadzu®, Milton Keynes, UK). According to ISO 527, moduli were measured at a constant speed of 1 mm min⁻¹ whilst tensile strengths and elongations at break were measured at 5 mm min⁻¹. Ten repeats for each category were achieved.

Significant differences were identified using an ANOVA technique. Mean comparisons by the Tukey–Kramer HSD method were made using JMP (SAS, Version 15.0.0, Marlow, UK). The criterion for showing significant difference between each pair is a p value below 0.05.

Differential Scanning Calorimetry (DSC)

DSC analyses were carried out using a Mettler Toledo DSC1 STAR^e system (Leicester, UK) on filaments of 10 mg to identify the PEKK grade. The polymer was tested by a dynamic scanning sequence

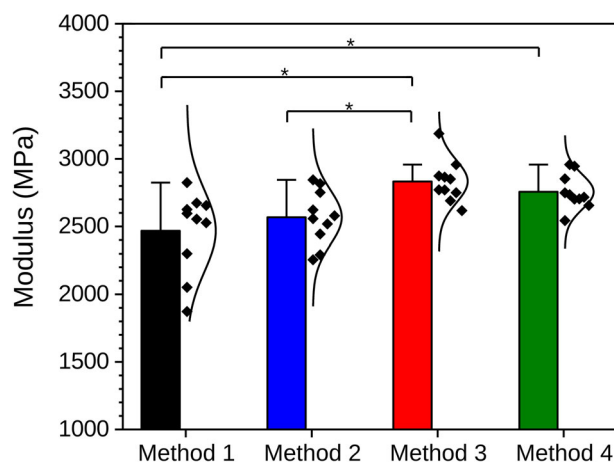


Figure 4. Tensile modulus for each method. Bar plots represent the mean values and the standard deviations. Normal distributions of all data points are also provided. Significant differences are indicated by the asterisk and brackets.

of two heating scans at 10 K min⁻¹ from 25 to 400 °C and one cooling scan at 10 K min⁻¹ from 400 to 25 °C. All scans were protected by a 50 mL min⁻¹ nitrogen flow.

RESULTS

The tensile modulus, tensile strength and elongation at break for each method are shown in Figs 4–6. The continuously connected specimens (method 3) returned the highest mean tensile modulus of 2833 MPa with a corresponding mean tensile strength of 38.6 MPa and a mean elongation of 3.9%. The individual specimens (method 1) returned the highest mean tensile strength of 53.8 MPa with a corresponding mean modulus of 2468 MPa and an elongation of 6.9%; however, both the modulus and elongation had a high standard deviation showing some variation.

The moduli of method 1 and method 2 specimens show overlapping results whilst the method 3 and method 4 specimens exhibited a significant shift to a higher modulus. The tensile strength shows a clearer grouping, with the method 2, method 3, and method 4 specimens showing a mean strength of 42.7 MPa, 38.6 MPa and 27.9 MPa respectively and the method 1 samples showing a significantly higher mean strength of 53.8 MPa.

The elongation follows a similar trend to the strength, where the method 1 and method 2 specimens show relatively higher mean values of 6.9% and 5.8% respectively and the method 3 and method 4 specimens show lower mean values of 3.9% and 3.0% respectively.

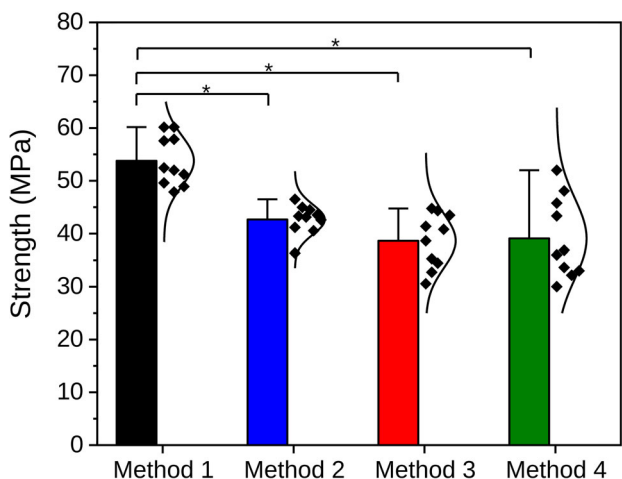


Figure 5. Tensile strength for each method. Bar plots represent the mean values and the standard deviations. Normal distributions of all data points are also provided. Significant differences are indicated by the asterisk and brackets.

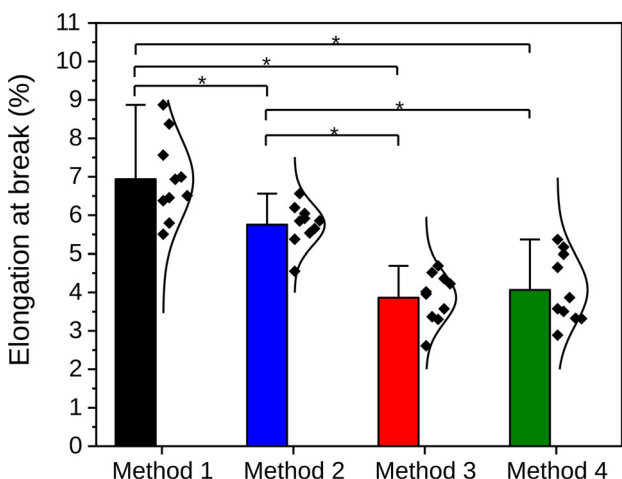


Figure 6. Elongation at break for each method. Bar plots represent the mean values and the standard deviations. Normal distributions of all data points are also provided. Significant differences are indicated by the asterisk and brackets.

DISCUSSIONS

PEKK grade and TTT diagram

The crystallisation speeds of PEKK materials are known to be determined by their various *para/meta* phenyl isomer ratios, more commonly known as the T/I ratios.¹⁹ The T/I ratio of Kimya PEKK-A filament was identified based on the DSC analysis. The melting points extracted from the thermogram are 306.5 °C in the first heating ramp and 311.2 °C in the second heating ramp, matching well the melting temperature of PEKK with a T/I ratio of 60/40,²⁰ as can be seen in Fig. 7(a).

The crystallisation behaviour of PEKK (60/40) has been investigated extensively.^{21,22} The time–temperature–transformation (TTT) diagram of PEKK (60/40) developed by Choupin *et al.*²¹ is partially displayed in Fig. 7(b). The TTT diagram reveals that PEKK (60/40) has the highest crystallisation speed at 230 °C. Even under this temperature condition, it still requires 150 s to initiate the crystallisation (i.e. reaching 1% crystallinity), which suggests that PEKK (60/40) is a slow crystallising grade compared with other semicrystalline PAEK grades.²³ Therefore, it is safe to conclude that all layer times in this printing matrix are too short to start crystallisation. In addition, visual inspection of all specimens confirms that they remain amorphous. For this reason, amorphous molecular diffusion across the layers is considered as the major mechanism governing the interlayer bonding of all printed samples.

Mechanical variations

Typical stress–strain behaviour of each method is exhibited in Fig. 8(a). It is noted that all specimens fractured prematurely before yielding. In Z tensile specimens, all layers are constructed in the XY plane, making them perpendicular to the loading direction. Along the loading direction, the interlayer bonding is, in general, weaker than the material's bulk strength. Therefore, the reported tensile strength and elongation at break values signify the interlayer bonding strength rather than the bulk property.

The interlayer bonding strength is directly linked to the level of molecular diffusion, which in turn is influenced by the local temperature near the interlayer surface. Once a new layer is deposited on top of a previous layer, thermally driven molecular motion prompts the amorphous molecular chains to diffuse across the layers. The diffusion process is temperature dependent: a high

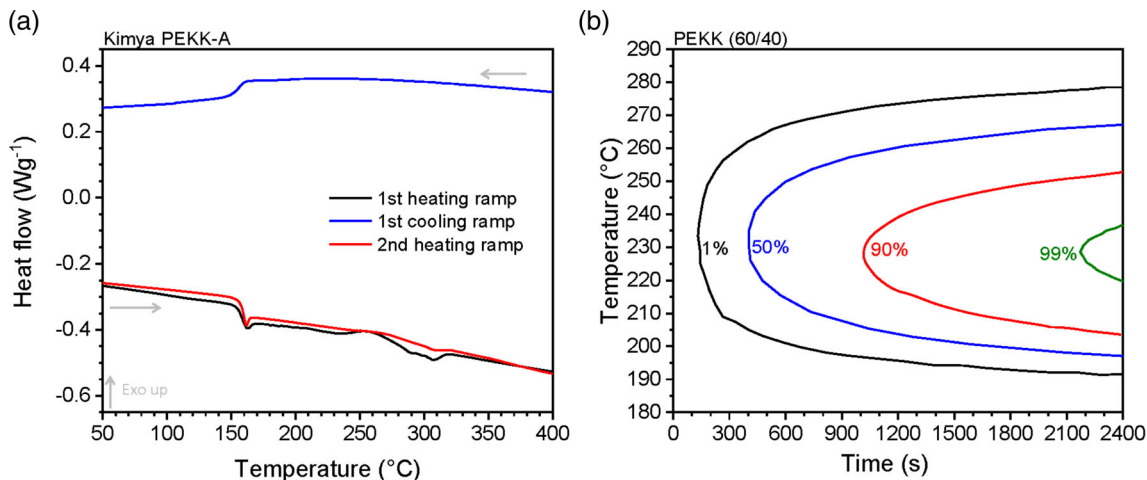


Figure 7. (a) DSC thermograms of Kimya PEKK-A. (b) TTT diagrams of PEKK with a T/I ratio of 60/40, adapted from reference 21.

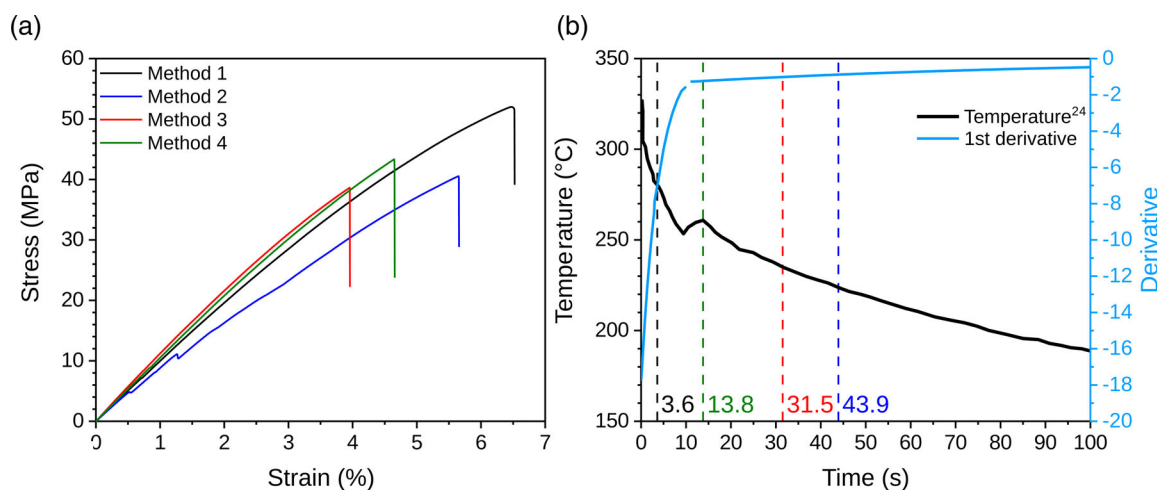


Figure 8. (a) Typical stress–strain curve of each method. (b) Temperature profile during FFF printing of PEKK components adapted from Lepoivre *et al.*,²⁴ with its first derivative and dashed lines indicating the gauge-length layer time of each method. The discontinuity at 10 s in the first derivative is caused by thermal fluctuation.

temperature promotes the diffusion, bringing a higher chance to achieve good interlayer bonding.

Meanwhile, the local temperature near the interlayer surface is determined by the layer time. Although the processing conditions (nozzle temperature, velocity, chamber temperature etc.) are kept constant for the fabrication of all specimens, the local conditions vary depending on the method of construction. Method 1 requires the nozzle to remain directly over the previously printed surface, further heating the polymer, with a very short layer time. In methods 2, 3 and 4, the nozzle moves away from previously printed material due to the larger cross-section and printing strategy, giving the previous layer longer time to cool without the heating effect created by the nozzle. The link between the layer time and the local temperature is evident: the shorter the layer time, the higher the local temperature.

To facilitate the discussion further, the temperature profile of printing PEKK measured by Lepoivre *et al.*²⁴ is shown in Fig. 8(b). In their study, the nozzle temperature was 356 °C, which is in a close range of the nozzle temperature (380 °C) used in the current study. Hence, the local temperature in this study is considered to follow the same trend as measured by Lepoivre *et al.*²⁴ The layer time in their study was 9.8 s, which explains the fluctuation of temperature profile observed around 10 s. To quantitatively investigate the rate of change in temperature between layers during cooling, the first derivative of the temperature profile was calculated. The derivative values highlight a significant change in slope up to approximately 10 s which could represent the critical layer time where mechanical differences will become substantial. This observation implies that, when layer time is longer than 10 s, the level of diffusion becomes less sensitive to the effect of layer time than when layer time is less than 10 s. The insensitivity explains why the strengths of specimens from methods 2, 3 and 4 are not significantly different, and why method 1 prints specimens with higher tensile strength and high elongation at break value than the other methods.

It is interesting to notice that the tensile moduli of specimens from methods 3 and 4 are generally higher compared with those of specimens from methods 1 and 2. As the crystallinity effect has

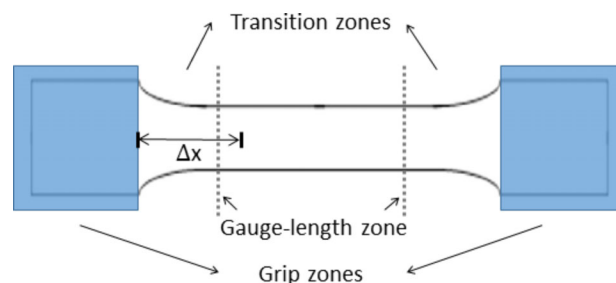


Figure 9. Illustration of the five zones of a dogbone tensile specimen. Δx marks the distance starting from the onset of the transition zone towards the gauge-length zone.

been ruled out, the cause of the change in modulus is not clear at this stage.

Fracture location

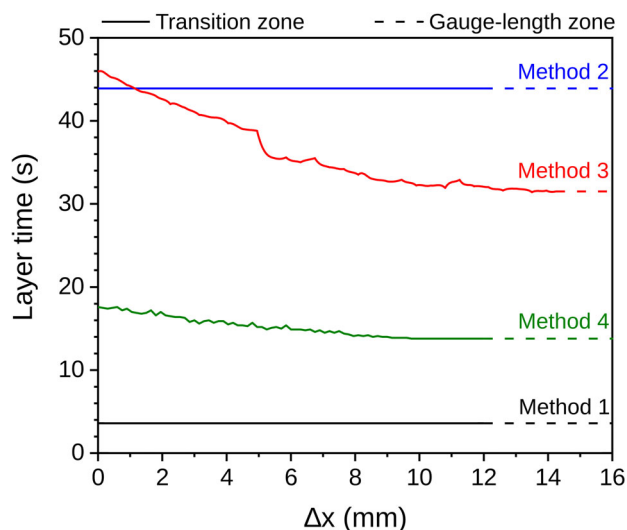
A dogbone shaped tensile specimen consists of five zones: two grip zones, two transition zones and one gauge-length zone (Fig. 9). In the tensile test, the dogbone shaped specimen is adopted to confine the deformation to the narrow parallel centre region (i.e. the gauge-length region) and to reduce the likelihood of fracture occurring outside this region. This is favoured because failure in the transition zones or in the grip zones would cause an improper measurement of the elongation values.

The fracture locations of all FFF specimens were documented and are summarised in Table 2. The distribution of fracture location varied according to the printing method. To investigate the potential cause of this distribution, layer times throughout the transition zone to the onset of the gauge-length zone for all methods were collected and are presented in Fig. 10.

The majority of method 2 specimens fractured in the gauge-length zone, behaving the same as conventional tensile specimens, e.g. made by injection moulding. Method 2 ensures the same layer time of 43.9 s across the whole specimen, resulting in the same level of interlayer bonding in the transition zone and in the gauge-length zone. Upon loading, the axial stress follows $\sigma_z(\text{transition zone}) < \sigma_z(\text{gauge-length zone})$ due to the fact

Table 2. Fracture location of tensile specimens from all methods

Method	No. of samples that break within the gauge-length zone	No. of samples that break in the transition zone
Method 1	3	7
Method 2	9	1
Method 3	5	5
Method 4	5	5


Figure 10. Layer time as a function of Δx (entire transition region). Δx is defined in Fig. 9 and marks the distance starting from the onset of the transition zone towards the gauge-length zone.

that the applied force is the same whilst the cross-sectional area increases in the transition zone. The higher axial stress in the gauge-length zone helps constrain the fracture to within this region. In addition, the smooth surface produced by cutting the sample out removed the stepping effect caused by building it in layers, minimising defects which can otherwise cause the sample to fracture in the transition region.

The fracture locations of method 3 and method 4 specimens are somehow arbitrary: half of them broke in the transition zone whilst the other half broke in the gauge-length zone. The fracture in the transition zone is potentially caused by two main factors. The first factor is the changing layer time. Relatively longer layer times in the transition zones bring lower local temperature, producing diffusion inferior to that in the gauge-length region. The second factor is the stepping surface finish in the transition zone. As FFF is a layer-by-layer manufacturing technique, the method 3 and method 4 specimens have a 0.15 mm stepping in the curves of the transition zone. These steps may act as defects causing fracture in the transition region. Closer inspection of the toolpath information generated by the slicing software showed no variation in the extrusion strategy between the gauge-length layers and the transition area layers; therefore advanced slicer settings influenced by overhanging geometry can be excluded.

More than half of method 1 specimens broke in the transition zone, probably due to the aforementioned stepping effects.

Surprisingly, the layer time of method 1 in the transition zone is constant around 3.6 ± 0.1 s, possibly due to the small cross-sectional area, so that the majority of the time was in the period that the nozzle was positioning itself (acceleration and deceleration phase) and not printing. Therefore, for method 1, the change in printing area for each layer is not reflected in the layer time as it is a small proportion of it.

CONCLUSIONS

Individually printed, machined, large and small connected type vertical FFF specimens were evaluated to quantify the mechanical variance between the four printing methods. Different methods lead to different layer times, causing various local temperature values near the interface. The strength and the elongation at break are found to be linked with the interlayer bonding strength. Slow crystallising Kimya PEKK-A was selected as the printing material to exclude the effect of crystallisation on the interlayer bonding strength, leaving the temperature-dependent amorphous molecular diffusion across the layers as the governing mechanism. A maximum, mean tensile strength of 53.8 MPa was observed for method 1 specimens, owing to the high level of diffusion induced by the very short layer time. The strengths of specimens printed via method 2, method 3 and method 4 are less sensitive to the effect of layer time, due to the decreasing spontaneous cooling rate. Moreover, the fracture locations indicate that the effect of surface finish and the changing layer time bring instability to the testing. Thus, standardising the Z tensile methodology (number of samples, layer time etc.) is desirable to the AM community so that datasets produced are comparable, with the right method selected to make it representable to likely printing processes, desired printed component layer time and part production. Additionally, full details should be provided in relation to the printing and testing methods to allow interested parties to make informed decisions on the performance of materials and printers.

REFERENCES

- Wohlers, T. T., & Wohlers Associates. (2012). Wohlers report 2012: Additive manufacturing and 3D printing state of the industry : annual worldwide progress report. Fort Collins, Col: Wohlers Associates.
- Popescu D, Zapciu A, Amza C, Baciu F and Marinescu R, *Polym Test* **69**:157–166 (2018).
- Mohamed OA, Masood SH and Bhowmik JL, *Adv Manuf* **3**:42–53 (2015).
- Dey A, Yodo N, *Journal of Manufacturing and Materials Processing*. 2019; **3**(3):64–93.
- Jaisingh Sheoran A and Kumar H, *Mater Today Proc* **21**:1659–1672 (2020).
- Berretta S, Davies R, Shyng YT, Wang Y and Ghita O, *Polym Test* **63**:251–262 (2017).
- Stratasys. Available: <https://www.stratasys.com/materials/search/ultem1010> [7 October 2020].
- Luvocom. Available: https://www.luvocom.de/fileadmin/user_upload/luvomaxx/Bilder/Produkte/LUVOCOM-3F-PET-CF-9780-BK.pdf [7 October 2020].
- International Organization for Standardization. (2012). Plastics-Determination of Tensile Properties, Part 2: Test Conditions for moulding and extrusion plastics. (ISO Standard No. 527-2).
- Stratasys. Available: https://www.stratasys.com/-/media/Files/Brochures/BR_FDM_MaterialsTestingProcedure_0919a [7 October 2020].
- Intamsys. Available: <https://www.intamsys.com/wp-content/uploads/2018/06/INTAMSYS-PEKK.pdf?t=1529919389> [7 October 2020].
- 3Dgence. Available: <http://support.3dgence.com/materialy.html> [7 October 2020].
- Gebisa AW and Lemu HG, *Procedia Manuf.* **30**:331–338 (2019).
- Wu W, Geng P, Li G, Zhao D, Zhang H and Zhao J, *Materials (Basel)* **8**:5834–5846 (2015).

- 15 Zhao Y, Chen Y and Zhou Y, *Mater Des* **181**:108089 (2019).
- 16 Rinaldi M, Ghidini T, Cecchini F, Brandao A and Nanni F, *Compos Part B Eng* **145**:162–172 (2018).
- 17 Arif MF, Kumar S, Varadarajan KM and Cantwell WJ, *Mater Des* **146**:249–259 (2018).
- 18 Zanjanijam AR, Major I, Lyons JG, Lafont U and Devine DM, *Polymers (Basel)* **12**:1665–1693 (2018).
- 19 Gardner KCH, Hsiao BS, Matheson RR and Wood BA, *Polymer (Guildf)*. **33**:2483–2495 (1992).
- 20 Arkema. Available: <https://www.extremematerials-arkema.com/export/sites/technicalpolymers/.content/medias/downloads/brochures/kepstan-brochures/kepstan-pekk-web.pdf> [7 October 2020].
- 21 Choupin T, Fayolle B, Régner G, Paris C, Cinquin J and Brulé B, *Polymer (Guildf)* **111**:73–82 (2017).
- 22 Benedetti L, Brulé B, Decraemer N, Davies R, Evans KE and Ghita O, *Addit Manuf.* **36**:101540 (2020). <https://doi.org/10.1016/j.addma.2020.101540>.
- 23 Tardif X, Pignon B, Boyard N, Schmelzer JWP, Sobotka V, Delaunay D *et al.*, *Polym Test* **36**:10–19 (2014).
- 24 Lepoivre A, Boyard N, Levy A and Sobotka V, *Procedia Manuf* **47**:948–955 (2020).